Presented at the 36th European PV Solar Energy Conference and Exhibition, 9-13 September 2019, Marseille, France

INDUSTRIALIZATION OF RIBBON INTERCONNECTION FOR SILICON HETEROJUNCTION SOLAR CELLS WITH ELECTRICALLY CONDUCTIVE ADHESIVES

Torsten Geipel[1], Veronika Nikitina[1], Luciana Pitta Bauermann[1], Esther Fokuhl[1], Erdmut Schnabel[1], Denis Erath[1], Alexander Krieg[1], Achim Kraft[1], Thomas Fischer[2], Robert Lorenz[2], Dieter Breitenbücher[2]
[1] Fraunhofer Institute for Solar Energy Systems ISE, Heidenhofstr. 2, 79110 Freiburg, Germany
[2] teamtechnik Maschinen und Anlagen GmbH, Planckstr. 40, 71691 Freiberg am Neckar, Germany
torsten.geipel@ise.fraunhofer.de

ABSTRACT: The use of electrically conductive adhesives (ECAs) and ribbons is a cost-efficient solution for the interconnection of silicon heterojunction (SHJ) solar cells already implemented in fully automated stringing equipment. A better understanding of the materials, the interconnection process and the reliability of the modules is still required. In this paper we present results of this interconnection approach focusing on material level, string production and performance analysis in outdoor operation. Firstly, the curing of ECAs is investigated. Furthermore, the volume and contact resistivity initially and after aging is characterized. ECAs in combination with Ag-coated and bare Cu ribbons are processed on an industrial glue stringer *TT1600ECA* from teamtechnik GmbH to manufacture SHJ solar cell strings. The uniformity of the cured bond line thickness is analyzed with optical microscopy. The bond line thickness is 32 to 38 µm on the sunny side. The peel force is characterized and the strings are further encapsulated in modules to test reliability and outdoor performance. The peel force ranges from 0.5 N mm^{-1} to 1.0 N mm^{-1} for certain ECAs. Adequate material combinations for PV modules showed degradation lower than 5% even in extended thermal cycle and damp heat testing. The outdoor test of SHJ modules over one year showed a 2% to 3.5% higher specific energy yield compared to a PERC reference module due to the absence of p-type related light induced degradation and a lower temperature coefficient of SHJ cells. With this work we contribute to the industrialization of ECA technology for SHJ cells by addressing relevant aspects of mass production.
Keywords: PV Module, Module Integration, Heterojunction, Electrical Properties, Screen Printing, Ribbons, Reliability

1. INTRODUCTION

Silicon heterojunction (SHJ) solar cells based on amorphous silicon thin films and crystalline silicon wafers with front and rear metallization achieve conversion efficiencies between 22% and 24% on industrial scale today [1]. The often observed low adhesion of the metallization to the wafer poses significant challenges to the cell interconnection process [2]. Currently, a few solutions for module integration are suggested: *Smart Wire Connection Technology* (SWCT) [3], the *NICE* approach [4], and fully-automated ribbon stringing with electrically conductive adhesives (ECAs) [5]. The latter has the advantage of being closer to the conventional interconnection process. Furthermore, the flexibility in the choice of ribbons and ECAs secure a steady, independent and cost competitive production. This paper highlights results of the publicly funded project *KleVer* conducted by teamtechnik GmbH and Fraunhofer ISE.

For the industrialization of ECA-based silicon heterojunction (SHJ) cell interconnection we performed work using the following techniques and equipment:

- characterization and simulation of the cure process,
- electrical characterization of ECAs,
- SHJ cell interconnection at an industrial stringer *TT1600ECA* with successive characterization of peel force and the microstructure of the bond,
- reliability tests of one-cell and 60-cell modules,
- outdoor monitoring of 60-cell modules over one year.

The results of the joint project with teamtechnik GmbH have helped to commercialize the ribbon-based ECA interconnection and module integration of SHJ cells [6,7].

2. MATERIALS AND METHODS

2.1. Electrically Conductive Adhesives (ECAs)

ECAs are polymeric glues filled with metallic particles. For Ag-filled isotropic ECAs the filler content is between 25 to 30%vol. to overcome the *percolation threshold* [8]. Not only pure Ag but also Ag-coated Cu particles are relevant fillers nowadays [9]. Typical base polymers are epoxies, acrylates or silicones, and also hybrid polymers are possible [10]. They become conductive after curing and crosslinking of the polymer with heat. The shrinkage of the polymeric matrix and the removal of lubricants surrounding the metallic particles are said to determine the conductivity of the ECA [11,12]. Detailed information on basic principles can be found in textbooks or review articles [8,13–18].

ECAs have been used at lab scale for the interconnection of silicon wafer H-pattern solar cells mainly motivated by an anticipated reduction of the cell thickness [19]. ECAs played a role in thin-film photovoltaic (PV) module production [20,21]. Additionally, they gained importance for the interconnection of back-contact solar cells [22]. In latest PV module developments, the shingle-type cell interconnection relies on the use of ECAs [23–25].

Many different commercially available ECA products and product revisions have been tested throughout the project. For the manufacturing tests, a selection of five different materials was made, which are summarized in Table II. The selection was based on prior experience with the ECA vendor, on the results of initial material characterization, practical considerations to limit the total test effort, but also reasonable price expectations (< 1000 €/kg). For some experiments not all materials were available at that time which is why certain data points are missing.

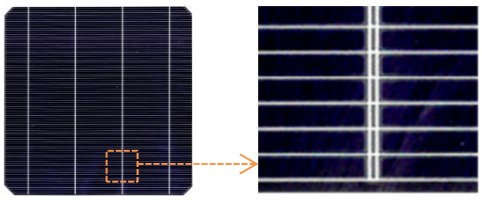

Figure 1: *Glue busbar* of SHJ cells

Figure 2: Stringer *TT1600ECA* at Fraunhofer ISE

2.2. Silicon Heterojunction Solar Cells

The bifacial, rear-emitter, M2 format, n-type, industrial SHJ cells were supplied by an external partner. Instead of regular busbars, the front side metallization features four pairs of fingers in a distance of 0.8 mm (*glue busbars*) instead of regular busbars (see Figure 1). These *glue busbars*, originally proposed in *ref.* [26], facilitate the I-V measurement at cell level with pins instead of wires, constrain the *bleed-out* of resin from the ECA (*cf.* [27]) and allow additional lateral conductivity, especially at the cell edges. Approximately 100 mg Ag per cell is saved by using *glue busbars* instead of regular busbars.

2.3. Stringer

The ECA stringer *TT1600ECA* is commercially available from teamtechnik GmbH (*see* Figure 2) [28]. The prototype machine at Fraunhofer ISE can be flexibly configured for conventional soldering with infrared light or ECA application. The stringer is capable of processing full and half cells with three, four and five busbars and shingle cells. The ECA is applied by screen printing. Curing is done with IR lamps and hot plates. The capability of the current stringer is 2.3 s per cycle, which represents a throughput of 1600 cells per hour.

2.4. PV Module Materials

The SHJ cells were encapsulated in a glass-backsheet configuration. For the one-cell modules a 3.2 mm glass pane without anti-reflection-coating was used whereas the glass for the 60-cell modules contained an anti-reflection coating. Both types of encapsulants used for the SHJ modules were polyolefin elastomers (POE). Furthermore, the backsheet was white PET/Al/PET.

The ribbons used to interconnect the SHJ cells were commercially available and made of a Cu core in the dimension (1.2×0.2) mm². They were coated with approximately 1 µm of Ag, but ribbons without Ag coating (bare Cu) were investigated as well. The ribbons featured a grooved structure to increase the internal light reflection in the module leading to 2% to 3% increase in short circuit current compared to conventional flat ribbons [29,30].

2.5. Peel Test

A 90° peel test was performed to study the mechanical strength of the interconnection in accordance with DIN 50461 [31]. A Zwick/Roell universal testing machine with a constant traverse speed of 50 mm min^{-1} was used. The recorded data, force over peel distance, is normalized to the ribbon width.

2.6. Cure Kinetic Simulation

The proper curing of the ECA is extremely important for adequate mechanical strength and good electrical properties of the interconnection joint. In a previous publication we experimentally investigated the relationship between curing conditions and peel force [32]. In this work, the cure kinetics of the ECAs was analyzed with differential scanning calorimetry (DSC) and additional simulation. The models described in our previous publication (*cf.* [33]) were improved by removing the assumption of a cure reaction model $f(\alpha)$. Since the model presented here is more generally applicable, it allows the simulation of a wider range of ECAs.

The time t_α to reach a degree of cure α at a constant absolute temperature T_0 is expressed as [34]

$$t_\alpha = \frac{\frac{1}{\beta}\int_0^{T_\alpha} \exp\left(\frac{-E_\alpha}{RT}\right) \mathrm{d}T}{\exp\left(\frac{E_\alpha}{RT_0}\right)} \quad (1)$$

The expression β is the constant heating rate of the DSC measurement of the uncured ECA, T_α is the absolute temperature at the degree of cure α during that DSC measurement, E_α is the activation energy of the cure reaction at α, R is the general gas constant, and T is the absolute temperature during the DSC measurement.

Various methods are available to determine E_α from which we frequently used the expression from Coats and Redfern [35]

$$\ln\left(\frac{\beta_\mathrm{i}}{T_{\alpha,\mathrm{i}}}\right) = \mathrm{Const} - \frac{E_\alpha}{RT_{\alpha,\mathrm{i}}} \quad (2)$$

In eq. 2, β_i is the constant heating rate for multiple DSC measurements of the uncured ECA, and $T_{\alpha,\mathrm{i}}$ are the absolute temperatures when achieving a fixed degree of cure α during the i-th DSC measurement. Plotting the left side of eq. 2 versus $(T_{\alpha,\mathrm{i}})^{-1}$ yields a straight line with the slope leading to E_α.

The curing of the ECA in the stringer takes place at an inconstant temperature $T(t)$. In this case, eq. 1 needs to be successively solved for many discrete T_0 values that approximate $T(t)$.

2.7. Electrical Characterization

The volume resistivity ρ_V of the ECA as a material property and the contact resistivity to various surface metals $\rho_{\mathrm{C,X}}$ (with X being Ag, Cu or Sn) determine the electrical properties of the interconnection. Sample preparation and the measurement of these properties is described in a previous publication [36]. It was shown that ρ_V should remain below 1×10^{-3} Ω cm and $\rho_{\mathrm{C,X}}$ should remain below 0.1 mΩ cm² to not affect the *FF* of the module.

The volume resistivity samples were treated with a damp heat (DH) test (+85 °C at 85% r.h.) for 1000 h without encapsulation. The contact resistivity samples (*cf.* Figure 3) were laminated using a microscope slide as a front glass (75 × 25 × 1) mm³, ethylene-vinyl-acetate (EVA) as an encapsulant and a PVF-PET-PVF backsheet before the DH 1000 test.

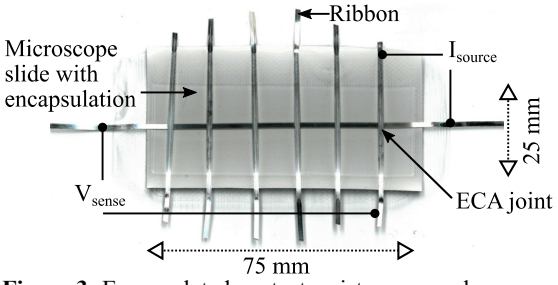

Figure 3: Encapsulated contact resistance sample

2.8. Reliability Tests and Outdoor Monitoring

We built one-cell modules of the ECA-ribbon combinations given in Table II in order to test DH and thermal cycling (TC) stability according to IEC 61215-2:2016 [37]. Furthermore, one 60-cell module with ECA A and with ECA E, both with bare Cu ribbons, were manufactured to test DH and successively TC at full-module scale. Note, that the one-cell modules were not current-loaded during the TC test in the climate chamber, whereas the 60-cell modules were. We reported about current-loaded DH tests of ECA-based modules in a previous publication [38].

Additionally, four 60-cell modules with the material combinations given in Table I were installed on a fixed outdoor rack tilted 45° to the south in Freiburg, Germany. IV curves, power and energy yield were monitored from May, 15th 2018 until July, 1st 2019.

Table I: Overview of 60-cell modules in glass-backsheet configuration with POE and Al-sealed white backsheet

No.	Cell	ECA	Ribbon	Test
1	SHJ	A	Ag	Outdoor
2 3	SHJ	A	Cu	Outdoor TC600+DH1000
4 5	SHJ	E	Cu	Outdoor TC600+DH1000
6	mono p-type PERC	-	Sn60Pb40	Outdoor

3. RESULTS AND DISCUSSION

3.1. Cure Kinetics of ECAs in the Stringer

Figure 4 shows the activation energy E_α of the cure process depending on the progress of the reaction. The data in Figure 4 was generated using DSC measurements at several constant heating rates and eq. 2. Except from start and end of the curing, ECA A, ECA B and ECA E seem to consist of a single step reaction. A relatively constant E_α is characteristic for this kind of process, whereas the deviations at start and end may likely be errors of the DSC measurement. However, the curing of ECA C and D is clearly characterized by a descending activation energy over the course of the reaction, which is indicative for a multiple step reaction [39].

The determined activation energies of the ECAs

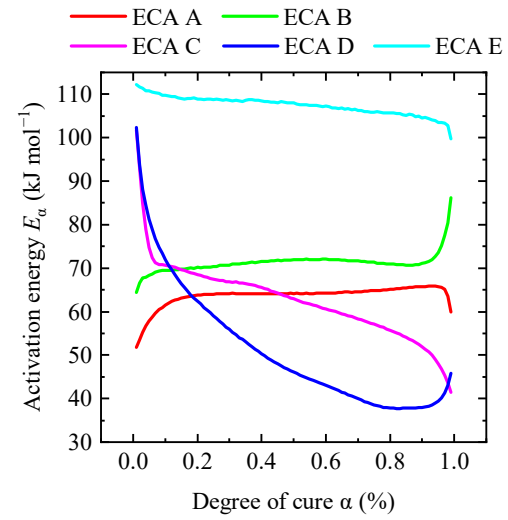

Figure 4: Activation energy of the curing process depending on the progress of the reaction (degree of cure)

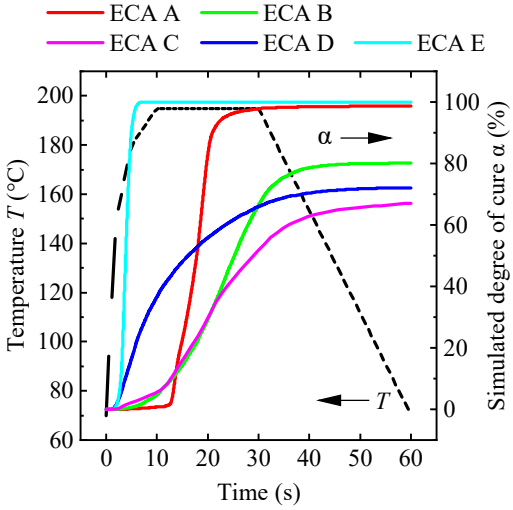

Figure 5: Temperature (black) and simulated degree of cure of ECAs

were used to simulate the degree of cure within the stringer. An approximated temperature profile $T(t)$ of the *TT1600ECA* stringer is shown in Figure 5 as a dashed line. It is shown in Figure 5 that ECA A and E are fully cured during the 30 s at the 195 °C hold temperature whereas ECA B, C and D achieve only 65 to 80% cure. A modification of the temperature profile for these materials (or the ECA chemistry) would be necessary to allow full cure. Using this simulation, we were able to discuss necessary improvements in the cure kinetics with the adhesive vendors or optimize the processes in the stringer.

3.2. Volume and contact resistivity

During the course of the project the volume resistivity of many ECAs has been characterized. A compilation of the results is given in Figure 6. Each data point in Figure 6 refers to a different ECA. The ECAs are sorted according to decreasing Ag content (datasheet values). The color and types of symbols denote the different types of base polymer.

An important observation from Figure 6 is that, regardless of the Ag content, ρ_V is often in the range between 1×10^{-4} and 1×10^{-3} Ω cm. Significant amounts of

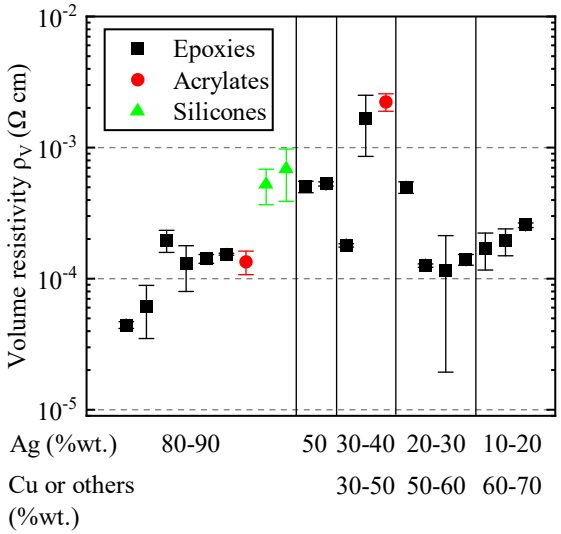

Figure 6: Volume resistivity of ECAs cured at 180 °C for 10 min sorted according to descending Ag content. Each data point refers to one ECA. The error bar denotes the statistical range of several measurements. The color and types of symbols (square, round, triangle) indicate different base polymers.

Ag can be replaced by Cu (Ag-coated Cu) or other metals without an increase in resistivity. This enables a cost reduction without sacrificing electrical performance. We did not observe a strong correlation of ρ_V to the base polymer although the two tested silicones were slightly higher in resistivity than most other ECAs. Nevertheless, these values are below the critical threshold of 1×10^{-3} Ω cm as previously recommended [36].

Volume resistivity samples without encapsulation were aged in DH 1000. The volume resistivity is shown in Figure 7. For ECA A, C, and D ρ_V does not change substantially. This is astonishing with regard to the harshness of the test. Only ECA E increased its resistivity by an order of a magnitude indicating degradation of the material. Visual inspection of the samples of ECA E after the DH test revealed ablated material from the microscope slide indicating embrittlement and loss of mechanical strength (*see* Figure 8).

The contact resistivity ρ_C of ECA A and E initially and after consecutive DH tests with encapsulated samples (*cf.* Figure 3) is presented in Figure 9a and b. Both ECAs possess an initial $\rho_{C,Ag}$ of averagely 3×10^{-4} mΩ cm². A soldered contact characterized equivalently has the same ρ_C. It is important to note that values published in literature can vary significantly due to the different methods used for the measurement and due to the fact that the contact resistivity is close to zero.

The initial contact resistivity $\rho_{C,Cu}$ is approximately

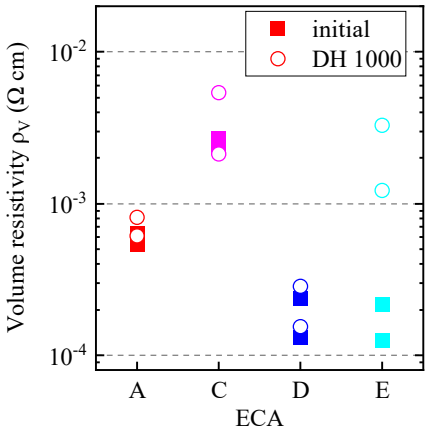

Figure 7: Volume resistivity of selected ECAs before (full) and after DH 1000 (open) (ECA B was not available at the time of testing)

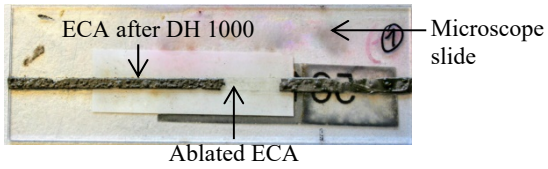

Figure 8: ECA E on a microscope slide after DH 1000 showing ablation of the material

6×10^{-4} mΩ cm² for ECA A and 3×10^{-2} mΩ cm² for ECA E. Obviously, ECA E is less suitable to be combined with Cu surfaces than ECA A, although the value obtained is still below the critical threshold of 0.1 mΩ cm² [36]. Hence, it is not expected that a difference in *FF* of the PV module is observed.

After DH aging we measured a tendency for an increase of ρ_C, in particular in the case of ECA A in combination with Cu and ECA E with both tested surfaces. It will be shown later that PV modules based on ECA A with Cu degrade less in DH than PV modules based on ECA E and Cu. Hence, if the contact resistivity measurement is used as a preliminary check of the stability in DH, these differences should be cautiously considered to anticipate a possible degradation.

3.3. SHJ Cell Interconnection

The selected ECAs are processed in accordance with Table II. In this experiment, full continuous ECA lines were printed. The laydown ranged between 40 to 85 mg per cell. The varying laydown of the ECAs was caused by the different metallic filler content (50–85 wt.%). The consumed ECA amount can be further reduced by almost 50% by using dotted printing [36]. Some ECAs are not further tested with Ag or Cu ribbons, be-

Table II: ECAs, process conditions and assessment of the printability, (†) Uncertainty is estimated to be ±2 mg

ECA	Ribbons tested	Printed amount (mg/cell)(†)	Printability	Cure temperature	Cure duration, machine cycle time
A	Ag-coated Bare Cu	40	Good	Const. 195 °C	30 s, 2.5 s/cycle
B	Ag-coated	40	Good	Const. 220 °C	60 s, 5 s/cycle
C	Bare Cu	60	Good	Up-down ramp with peak at 170 °C	30 s, 2.5 s/cycle
D	Ag-coated	85	Bad	Const. 220 °C	60 s, 5 s/cycle
E	Bare Cu	85	Good	Const. 160 °C	30 s, 2.5 s/cycle

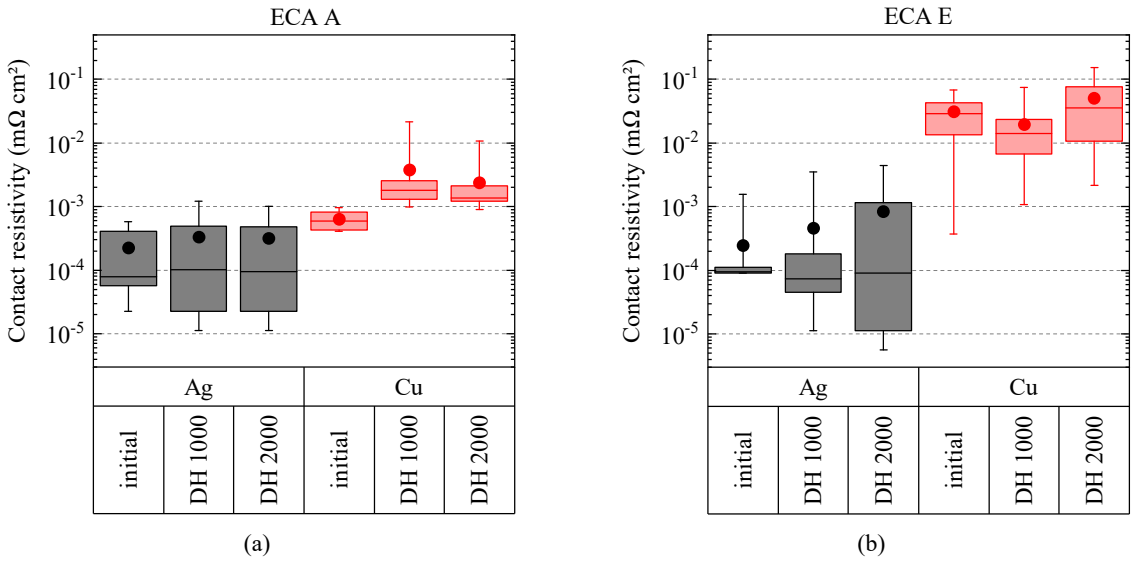

Figure 9: Contact resistivity of (a) ECA A and (b) ECA E before and after DH aging (box: 5-95% quantiles, line: median, circle: mean)

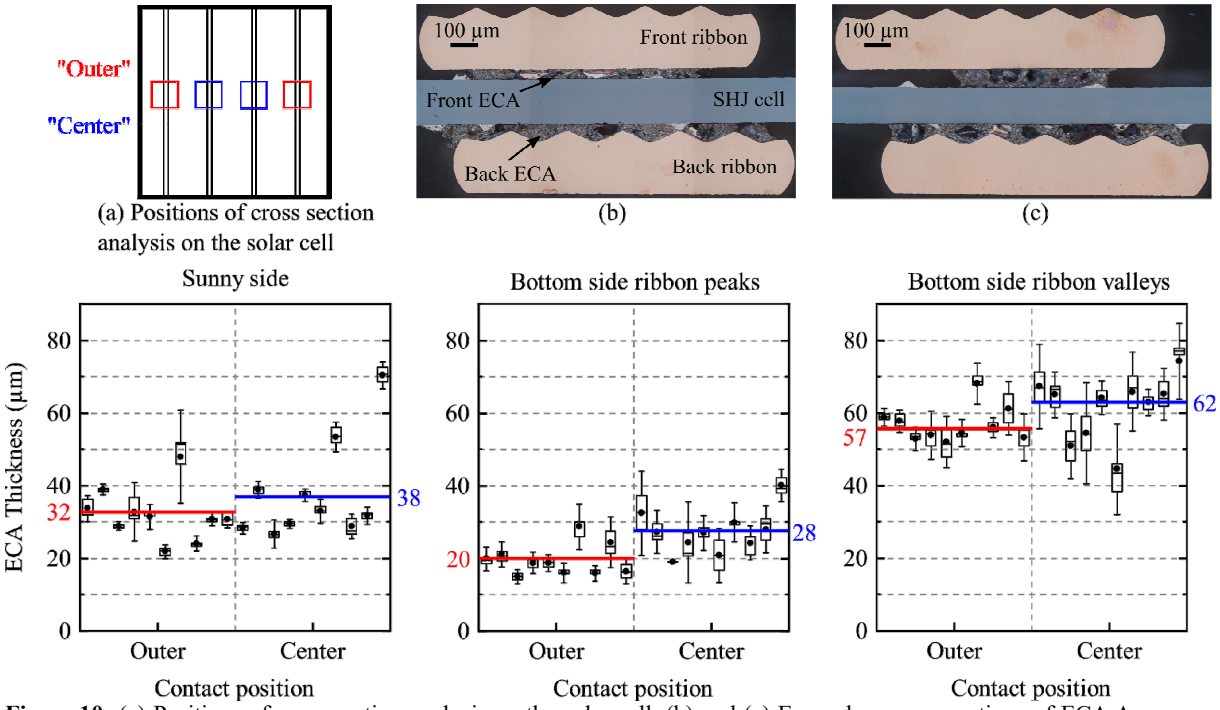

Figure 10: (a) Positions of cross section analysis on the solar cell. (b) and (c) Exemplary cross sections of ECA A connections and statistical analysis of thickness after curing.

cause one of each either showed no adhesion or was previously known to be electrically incompatible. The cure temperature profile needs to be adopted for each ECA (*cf.* Figure 5). Note that a maximum of 30 s total cure duration can be allowed for sufficient throughput.

The evaluation of printability in Table II is based on optical inspection of the uniformity and reproducibility of the print and the peel strength. Further details of the particular result of ECA D were previously published [32].

The wet laydown of 40 mg/cell of ECA A was uniform for several hours of production in the stringer. We quantified the homogeneity of the cured ECA thickness by means of optical microscopy of cross sections. Therefore, we measured the thickness of ECA A at two different positions of ten cells. The positions were *outer* and *center* (*cf.* Figure 10a). The cells were taken from the production run at the stringer in intervals of several minutes. Many cross sections resembled the microscopic image in Figure 10b. The front ribbon's structured surface directs to the sunny side. The back ribbon's structure is attached to the rear side of the cell. Due to this systematic non-uniformity it is important to ensure proper filling up the grooves with ECA at the rear. A slight misalignment of the ribbons between 100 to 200 µm was observed, which can be eliminated by fine tuning the ribbon placement in the stringer.

At the sunny side, the thickness was averagely 32 µm at the outer positions and 38 µm at the center positions. Most values range between 20 and 40 µm. At the

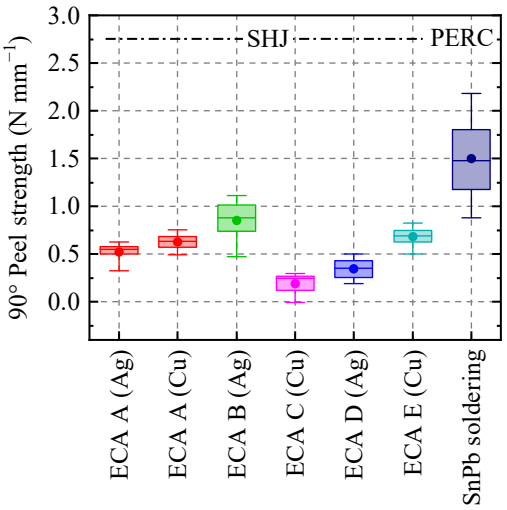

Figure 11: 90° peel force of ECA bonds after a production run at the *TT1600ECA*

rear side, the thickness, as measured from peak to cell surface, was 20 µm at the outer positions and 28 µm at the center positions. The corridor of values is approximately 15 to 35 µm. Considering the measurement from valley to cell surface at the rear side, we observed 57 µm at the outer positions and 62 µm at the inner positions. Most values were between 55 and 70 µm.

Occasionally, outliers with an increased thickness as shown Figure 10c were observed. The reason is a localized, insufficient down holding of the ribbon to the cell during the cure process. This was improved with a new down holder design by teamtechnik. Furthermore, the reason for the systematically higher thickness in the center positions was a slightly higher ECA print at the center due to a bending of the screen.

The ECA thickness varies considerably although the laydown is constant during the production. This may slightly influence the peel force over the length of the glue line. However, no influence on electrical performance or reliability is anticipated as long as a firm mechanical attachment is existent.

The 90° peel force after the production test is shown in Figure 11. ECA A, B and E achieved peel forces in the range between 0.5 to 1.0 N mm^{-1}. For reference, the peel force of a conventional solder connection on PERC cells with busbars is also given in Figure 11.

Usually the peel force of ECA interconnections is lower than that of solder contacts, due to the localized nature of peel stress, reduced toughness of polymers compared with metals and also caused by the metallic fillers [17]. Nevertheless, Hoffmann *et al.* showed that a peel force below 1 N mm^{-1} does not lead to failure in thermal cycling [40]. From our experience, a peel force of 0.5 N mm^{-1} is sufficient to allow a save handling of strings and to avoid mechanical damage of the interconnection before module lamination.

Sometimes we observed low peel strength when we used Ag-coated ribbons from a different batch of the same ribbon vendor. This occurred pronouncedly for ECA E which has, according to manufacturer information, a cationic cure mechanism. To date, we were not able to understand this phenomenon fully, although we checked organic contaminations on the surface, thickness of the Ag coating, and mechanical properties of the core.

We succeeded to produce strings, which were further processed into PV modules for reliability and outdoor monitoring. The 60-cell modules achieved a CTM ratio of P_{MPP} of 94–95%. It is noteworthy that modules made from Ag-coated ribbons and bare Cu ribbons obtained almost the same efficiency.

A significant contribution to the CTM loss arises from a high line resistivity of the fingers. The metallization (number of fingers and finger width) of the SHJ cells was originally designed for an interconnection with 18 wires. Hence, the distance of current flow in the fingers is significantly increased if only four busbars are used. The metallization at cell level can be optimized to suit to busbar interconnection. In a different project with optimized metallization for busbar interconnection we obtained a CTM ratio of 98.8% [41].

3.4. Module Reliability

SHJ one-cell modules with ECA-ribbon configurations of Table II were exposed to TC and DH tests. Figure 12a shows the relative power after TC 600. ECA A and B degrade by 2–3% in P_{MPP} on average, which is the same as the soldered references. ECA C, D and E degrade by more than 10% due to an incompatibility to Cu surfaces. We assume that the ECAs would not have de-

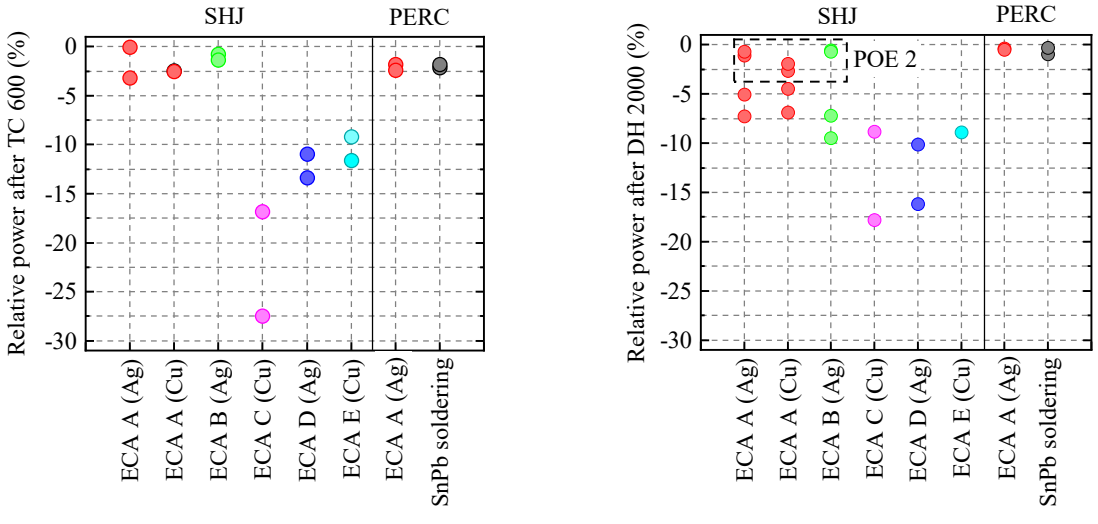

Figure 12: (a) Relative power of one-cell modules after TC 600, (b) after DH 2000. (No modules with POE 2 and ECAs C, D and E were built.)

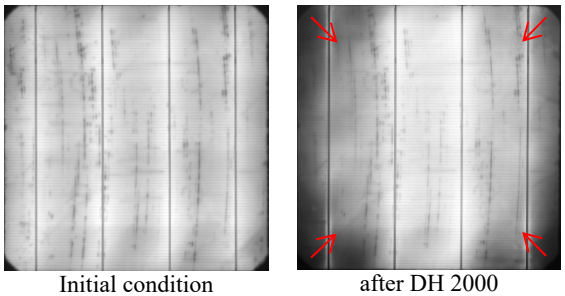

Initial condition after DH 2000

Figure 14: Electroluminescence images of one-cell module with ECA E before and after DH 2000 showing degradation at the edges resulting from humidity ingress

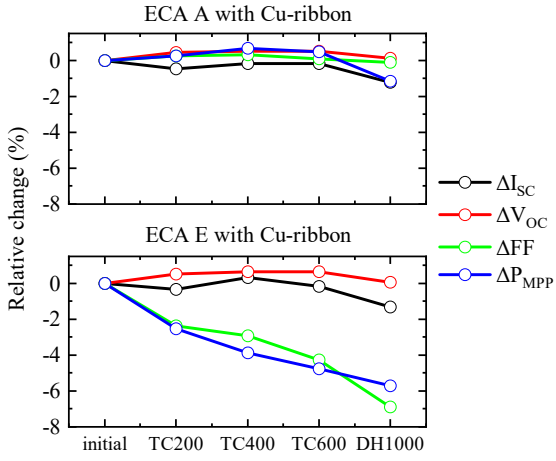

Figure 13: Results of the TC and successive DH tests with glued 60-cell SHJ modules using Cu ribbons

graded if combined with Ag-coated ribbons. The degradation of ECA D is probably the result of the improper printing as indicated in Table II.

The results of DH 2000 tests are shown in Figure 12b. Modules with ECA A and B decline in power by 6% on average and the remaining ECAs in a range of 10 to 20%. The degradation is caused by an assumed (but not finally clarified) sensitivity of SHJ cells to humidity. Although the rear of the module is completely sealed by the Al barrier in the backsheet, humidity can still enter from the sides (*see* Figure 14). The humidity ingress from the edges was prevented by changing the type of encapsulant to POE 2. Then, the degradation was limited to only 1−2.5% (results marked with a dashed rectangle in Figure 12b). Furthermore, the degradation can also be limited by using an edge sealing.

Two 60-cell modules were first tested in TC 600 and then with DH 1000. The results of measurements are shown Figure 13. The module made from ECA A with Cu ribbons showed a power loss of 1.2% after the entire sequence, whereas the module with ECA E and Cu ribbons dropped in P_{MPP} by 6.9%. The degradation of ECA E in combination with Cu ribbons was not unexpected if the characterization of the contact resistivity as shown in section 3.2 is considered. ECA E was conspicuous by having two orders of magnitude higher contact resistivity on Cu than on Ag-coated ribbons.

3.5. Outdoor Monitoring

Three SHJ modules and one soldered p-type mono PERC reference module in the configuration given in Table I were monitored in the field from May, 15th 2018 to July, 1st 2019. We considered the specific, cumulated yield relative to the soldered PERC reference module (Y_{rel}) that is expressed as:

$$Y_{rel} = \frac{\frac{Y}{P_{STC,indoor}}}{\frac{Y_{ref}}{P_{ref,STC,indoor}}} \quad (3)$$

Hereby, Y is the cumulated energy yield of the SHJ module (in kWh). $P_{STC,indoor}$ is the module power determined with the initial indoor measurement under standard test conditions (STC). Y_{ref} is the cumulated energy yield of the PERC reference module, and $P_{ref,STC,indoor}$ is the initial power of the PERC reference module under STC.

The characteristics of the SHJ modules were monitored during the outdoor exposure. We report them as values relative to the PERC reference module. The mathematical description is (taking for instance the *FF*):

$$FF_{rel} = \frac{\frac{FF}{FF_{STC,indoor}}}{\frac{FF_{ref}}{FF_{ref,STC,indoor}}} \quad (4)$$

The relative energy yield of the SHJ modules Y_{rel} over the course of one year outdoor exposure is shown in Figure 16a. The specific energy yield (kWh/kWp) of the glued SHJ modules was between 2 to 3.5% higher than a soldered PERC reference module. The main reason for the initial offset, marked as (I) in Figure 16a and b, is traced back to light induced degradation (LID) of the p-type PERC module in the first 20 to 40 hours of light exposure. LID of the p-type PERC reference module is likely to recover after the monitored one year exposure. Since the SHJ modules were made of n-type wafer material they do not suffer from this degradation mode.

Additionally, the glued SHJ modules possess a temperature coefficient of P_{MPP} of −0.34 % $K^{-1}$and the soldered PERC module has a temperature coefficient of P_{MPP} of −0.40 % K^{-1} (measurements made at ISE-Callab Modules). This gives SHJ modules an advantage during outdoor operation in particular if ambient temperature is high.

Besides the initial offset of specific yield there was a notable shift in the outdoor data between the points marked with (I) and (II). The SHJ modules increased in $P_{MPP,rel}$ by approximately 0.5% corresponding to an increase in FF_{rel} and $V_{OC,rel}$ of 0.5−1% as well as a slight decrease of $I_{SC,rel}$ of ~0.5%. There probably exists a positive light soaking effect of SHJ cells and modules during the first 150 h at 1-sun illumination [42,43].

Approximately in October 2018, marked as (III), a seasonal decline of SHJ module performance relative to the PERC modules set in. The decrease of $P_{MPP,rel}$ of the SHJ modules corresponded to a decrease in FF_{rel} and $V_{OC,rel}$ as well as an increase $I_{SC,rel}$. Furthermore, this decrease correlated to a reduction of module temperature during this period. This indicates that low operating temperatures level out the advantage of the temperature coefficient of the SHJ modules. However, in April 2019, when operating temperatures started to rise again (marked as (IV)), the $P_{MPP,rel}$ of the SHJ modules returned to their initial values from the beginning of the monitoring phase. Thus, in longterm operation a slight decrease of Y_{rel} during the colder months will likely be observed that will be returned in the warmer months.

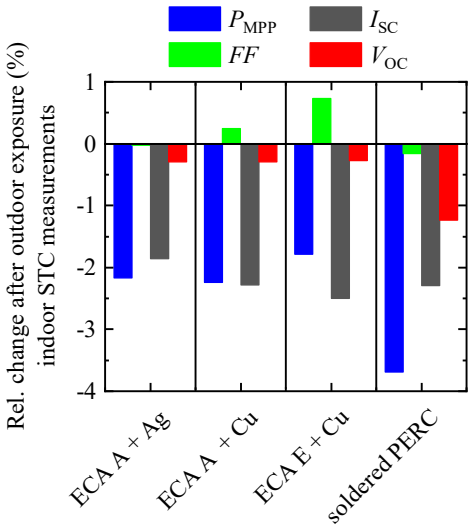

Figure 15: Relative change of parameters based on indoor STC measurements of modules installed on an outdoor test site for 12 months

If the indoor STC measurements before the installation of the outdoor test site and after finishing the monitoring phase are considered, the relative change of STC values, as shown in Figure 15, were obtained. A drop of I_{SC} of 2%, a tendency to increase in FF (0.5%) and a slight reduction of V_{OC} (0.2%) was measured with the SHJ modules that could correspond to the light soaking effect mentioned earlier [43]. The soldered PERC module lost 3.5% of P_{MPP}, 2% of I_{SC} and 1.2% of V_{OC}, which correlates to LID.

On the basis of this one year field test, we conclude that glued SHJ modules showed same or less degradation of performance compared to a soldered reference module. The n-type SHJ modules gained 2−3.5% higher specific energy yield in the field due to absent LID. Furthermore, we assume that the better temperature coefficient of SHJ technology gives an improved energy yield of 1% compared to the soldered PERC reference.

4. SUMMARY AND CONCLUSION

This paper presented results of the joint project *KleVer* between teamtechnik GmbH and Fraunhofer ISE in order to industrialize the interconnection of SHJ cells with ribbons and ECAs. The cure kinetics of the ECAs was simulated. It was shown that ECA A and ECE E achieved full cure during the process time of the stringer.

The characterization of volume resistivity of a wide range of ECAs showed that the Ag content can be reduced to ~20 wt% while keeping the resistivity lower than 1×10^{-3} Ωcm. We tested the stability of the volume resistivity during DH 1000 using samples without encapsulation. Despite these harsh conditions, the volume resistivity is barely affected except in one case.

Furthermore, we measured the contact resistivity of ECA A and E initially and after DH 1000 aging with encapsulated samples. The initial contact resistivity on Ag contacts is approximately 3×10^{-4} mΩcm² for both adhesives and the same as for soldered contacts; on Cu contacts it is one (ECA A) or two magnitudes (ECA E) higher. The contact resistivity tends to increase more for ECA E during successive DH aging.

Production tests with industrial SHJ cells including four *glue busbars* using a commercially available *TT1600ECA* stringer were performed. Five commercially available ECAs were tested, the amount of printed material was determined and the printing quality was evaluated. The amount of printed ECA (full line print) varies between 40 mg and 85 mg per cell (4BB) among the adhesives, because of the different filler content. ECA A and B achieve the lowest printing amount with 40 mg.

A microstructural analysis was made on cells with ECA A to analyze the uniformity of the bond line after cure. We found an average thickness at the sunny side of 32 µm. The outer busbars have on average a thickness of 38 µm. The thickness can vary between ±20 µm. Outliers in thickness existed where the downholder did not press tightly enough to spread the glue underneath the ribbon. This challenge was solved with an optimized version of downholder.

The 90° peel force of ECA A, B and E was between 0.5 N mm^{-1} and 1.0 N mm^{-1}, lower than for typical solder contacts, but in any way adequate for further string processing in production.

PV modules were fabricated for reliability and outdoor tests. One-cell modules with ECA A and B showed a degradation <3% in P_{MPP} after TC 600. The same ECAs and using an appropriate POE lead to 1.0−2.5% degradation in DH 2000 even without edge sealant. ECA A in combination with bare Cu ribbons showed stability in TC 600 and successive DH 1000 within a 60-cell module. The degradation of the module with ECA E correlated with increased volume and contact resistivity.

The one year outdoor monitoring with ECA-based, 60-cell SHJ modules yielded the following results: The SHJ modules achieved 2.0−3.5% higher specific yield relative to a p-type mono PERC reference during the monitoring period due to the absence of LID and the lower temperature coefficient of SHJ technology. The advantage of the temperature coefficient is a seasonal effect and diminishes in colder months. A final indoor characterization of the modules showed a lower degradation of the glued SHJ modules (−2%) compared to the PERC module (−3.5%).

During the project with teamtechnik GmbH we obtained a better understanding of ECAs and were able to trigger further technical improvements and cost reductions with the ECA vendors. We gained valuable experience with the production capability of these materials and showed good reliability and energy yield of certain materials and combinations.

ACKNOWLEDGEMENTS

This project was funded by the German Ministry for Economic Affairs and Energy within the research project *KleVer* under contract number 0325833. We thank teamtechnik GmbH for supporting this project.

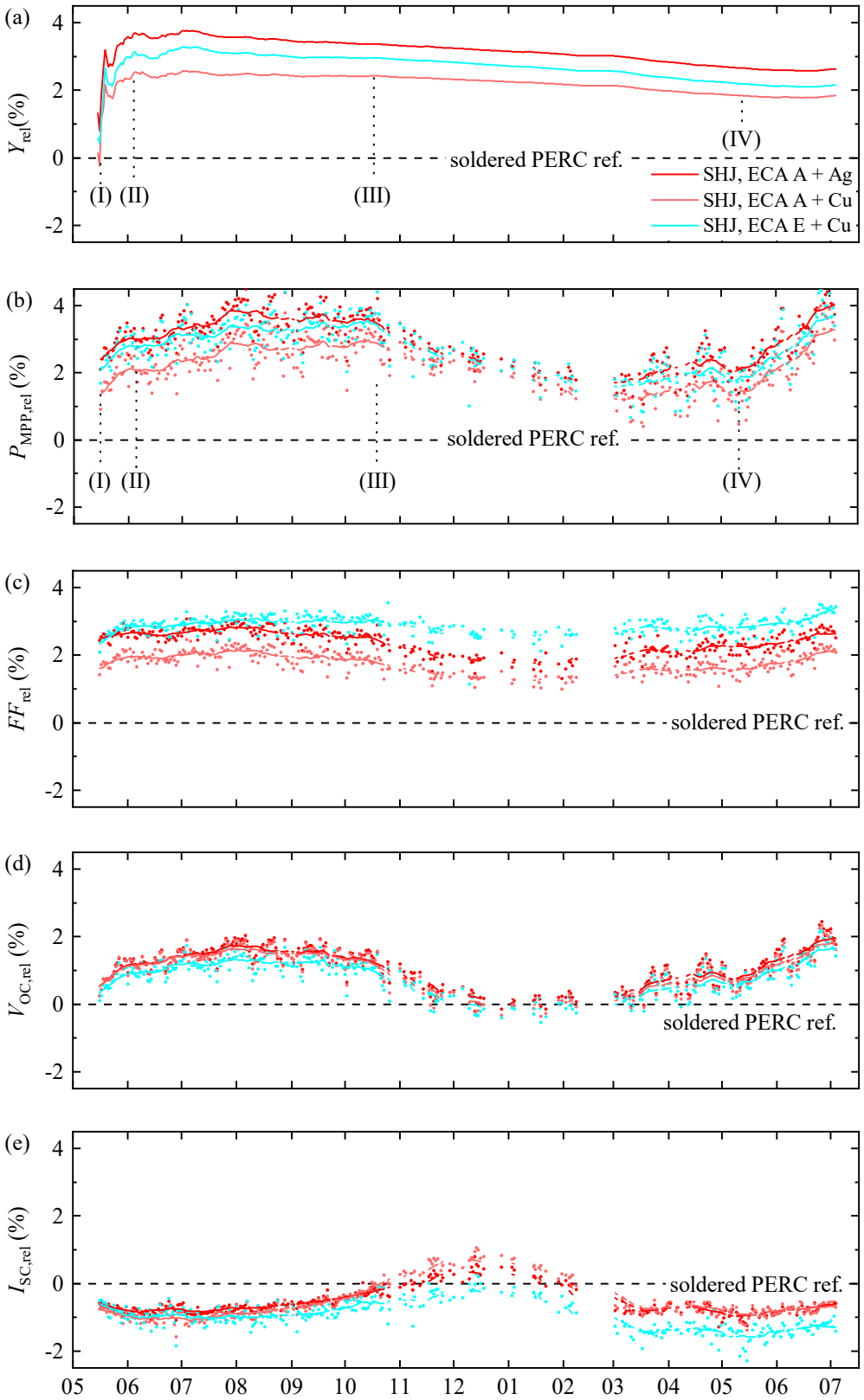

Figure 16: Field data of SHJ modules based on ECA technology compared to a soldered PERC reference module from May, 15th 2018 to July, 1st 2019

5. REFERENCES

[1] J. Zhao, *et al.* WCPEC-7, 45th IEEE PVSC, Waikoloa Village, HI, USA (2018), 1514–1519.

[2] A. De Rose, *et al.* 33rd EUPVSEC, Amsterdam (2017), 710–714.

[3] A. Faes, *et al.* 29th EUPVSEC, Amsterdam, Netherlands (2014), 2555–2561.

[4] D. Reinwand, *et al.* WCPEC-7, 45th IEEE PVSC, Waikoloa Village, HI, USA (2018), 628–631.

[5] teamtechnik Maschinen und Anlagen GmbH, Innovative adhesive technology for industrial serial production: Stringer TT1600ECA, available at https://www.teamtechnik.com/en/solar/stringer-tt/stringer-tt1600-eca/ (accessed on January 25, 2019).

[6] teamtechnik Maschinen und Anlagen GmbH, Lower costs, more efficiency: Russian module manufacturer and PV project developer Hevel LLC switches to adhesive technology from teamtechnik for its HJT modules (2018).

[7] teamtechnik Maschinen und Anlagen GmbH, Major contract for teamtechnik: Italian PV manufacturer orders stringers for production of high-efficiency modules with HJT cells (2018).

[8] G. Rabilloud, High-Performance Polymers - 1 Conductive Adhesives: Chemistry and Applications, Éditions Technip, Paris (1997).

[9] T. Geipel, M.Z. Huq, U. Eitner, Enrgy Proced 55 (2014), 336–341.

[10] A. Henckens, presentation held at the 3rd MWT workshop, Freiburg (2011).

[11] D.D. Lu, Q.K. Tong, C.P. Wong, IEEE Transactions on Components and Packaging Technologies 22 (1999), 365–371.

[12] D.D. Lu, C.P. Wong, International Journal of Adhesion and Adhesives 20 (2000), 189–193.

[13] D.D. Lu, C.P. Wong, in: D.D. Lu, C.P. Wong (Eds.), Materials for Advanced Packaging, Springer US, 2009, pp. 365–405.

[14] J.E. Morris, L. Wang, in: K.L. Mittal, T. Ahsan (Eds.), Adhesion in Microelectronics, John Wiley & Sons, Inc, Hoboken, NJ, USA, 2014, pp. 173–210.

[15] M.J. Yim, *et al.*, Journal of Adhesion Science and Technology 22 (2008), 1593–1630.

[16] M.J. Yim, K.W. Paik, Electronic Material Letters 2 (2006), 183–194.

[17] T. Geipel, U. Eitner, Photovoltaics International 21 (2013), 27–33.

[18] T. Geipel, Electrically conductive adhesives for photovoltaic modules. Dissertation, Hannover (2018).

[19] I.J. Bennett, *et al.* 22nd EUPVSEC, Milano (2007), 2674–2678.

[20] M. Pinarbasi, *et al.* 35th IEEE PVSC, Honolulu (2010), 169–174.

[21] R. Wells, Mark Francis, Southeast asia global solar technology 2 (2011).

[22] D.W.K. Eikelboom, *et al.* 29th IEEE PVSC, New Orleans (2002), 403–406.

[23] G. Beaucarne, Energy Procedia 98 (2016), 115–124.

[24] N. Klasen, *et al.*, in: 8th Workshop on Metallization, Constance, 2019.

[25] R. Morad, *et al. (*Congenra Solar, Inc.) Patent US 2015/0349190 A1, 2015.

[26] A. Schneider, *et al.*, Energy Procedia (Energy Procedia) 38 (2013), 387–394.

[27] M.L.D. Scherff, *et al.* 4th IEEE WCPEC, Waikoloa, Hawaii, USA (2006), 1384–1387.

[28] teamtechnik Maschinen und Anlagen GmbH, Innovative adhesive technology for industrial serial production: Stringer TT1600ECA, available at https://www.teamtechnik.com/en/solar/stringer-tt/stringer-tt1600-eca/ (accessed on January 25, 2019).

[29] E.M. Sachs, *et al.* 24th European Photovoltaic Solar Energy Conference, Hamburg (2009), 3222–3225.

[30] J. Schneider, *et al.*, Prog. Photovolt: Res. Appl. 22 (2014), 830–837.

[31] DIN EN 50461: 2007-03, Solarzellen - Datenblattangaben und Angaben zum Produkt für kristalline Silicium-Solarzellen (2007).

[32] A. De Rose, *et al.*, Photovoltaics International 40 (2018), 78–86.

[33] T. Geipel, U. Eitner, IEEE J. Photovoltaics 3 (2013), 1208–1214.

[34] S. Vyazovkin, Journal of Thermal Analysis and Calorimetry 83 (2006), 45–51.

[35] S. Vyazovkin, N. Sbirrazzuoli, Macromolecular Rapid Communications 27 (2006), 1515–1532.

[36] T. Geipel, *et al.*, IEEE J. Photovoltaics 8 (2018).

[37] IEC IEC 61215-2:2016, Terrestrial photovoltaic (PV) modules – Design qualification and type approval – Part 2: Test procedures (2016).

[38] L.P. Bauermann, *et al.*, Energy Procedia 124 (2017), 554–559.

[39] S. Vyazovkin, International Journal of Chemical Kinetics 28 (1996), 95–101.

[40] S. Hoffmann, *et al.* 33rd EUPVSEC, Amsterdam (2017), 183–186.

[41] A. De Rose, *et al.*, 2CO-11-4, this conference (2019).

[42] E. Kobayashi, *et al.*, Sol Energ Mat Sol C 173 (2017), 43–49.

[43] E. Fokuhl, *et al.*, 4BO.12.2, this conference (2019).